Adsorption 11: 467–471, 2005

Micropore Adsorption Dynamics in Synthetic Hard Carbons

GUDRUN REICHENAUER
Physics Department, Wuerzburg University, D-97074 Wuerzburg, Germany
reichenauer@physik.uni-wuerzburg.de

Abstract. The kinetics of the adsorption of CO_2 at 296 K in the micropores of sol-gel derived, monolithic carbons indicates two different types of micropores. While the micropore volume as well as the micropore width of both species turns out to be very similar, their accessibility is significantly different. To study the adsorption kinetics in more detail a set of sol-gel derived hard carbons was prepared with average macropore sizes ranging from about 50 nm to 5 micron at a total porosity of about 85%. To characterize the morphology of the samples small-angle X-ray scattering and N_2 sorption at 77 K were applied. Evaluation of the structural characteristics and the adsorption kinetics of the carbons investigated reveals that the two different types of micropores are homogeneously spread throughout the carbon backbone. The adsorption kinetics in the readily accessible type of micropores is dominated by the gas phase transport through the macropores combined with transport along the inner surface. In contrast, the access to the second category of micropores is highly restricted even at 296 K; this is reflected in equilibration times of about 500 s. The characteristics of the slow adsorption component is almost independent of the macroscopic size and the morphology of the specimen, suggesting that the slow kinetics is controlled by the local accessibility of the micropores. Surprisingly, the equilibrium data of the two adsorption components as a function of the relative pressure reveal that the micropores that are only slowly filled are actually characterized by a lower (Dubinin-Raduskevich) energy and thus a larger micropore width than the ones that are readily filled. This can be interpreted in terms of micropores with a very narrow entrance (restricted diffusion) or a widening of the micropores due to swelling of the carbon upon CO_2 adsorption.

Keywords: adsorption, micropores, restricted diffusion, kinetics, carbon

1. Introduction

Several authors report on a two step adsorption behavior of CO_2 in the micropores of carbons [1–4]; hereby the characteristic times for the contribution with the slower adsorption kinetics are found to range from several minutes to more than a week.

Amorphous carbons are important materials for many applications such as electrochemical devices, catalyst supports, adsorbers in filter systems and gas separation. In all cases, the design of their microporosity is one of the key parameters. For example for gas separation, both, the equilibrium sorption properties of the carbon as determined by the number and size of the micropores, as well as the kinetics of adsorption in these micropores can be exploited (Yang et al., 1997).

Slow kinetics for the diffusion of CO_2 and other gases into micropores of phenolic-based resins have been reported by Alcaniz-Monge et al. (2002) and Przepiorski et al. (2002). Depending on the adsorptive/adsorbate combination equilibration times ranging from several seconds up to more than a week have been observed: Nakashima et al. (1995) detected a two-step adsorption process for CO_2 in phenolic based carbon beads pyrolized at 1000°C; about 40% of the total amount was adsorbed readily within the first 10 min after dosing, while for the residual 60% it took up to 200 hours to reach adsorption equilibrium. The authors interpreted the latter effect as diffusion into micropores through narrow restrictions.

Carbon aerogels are resorcinol-based, synthetic, monolithic hard carbons, consisting of a

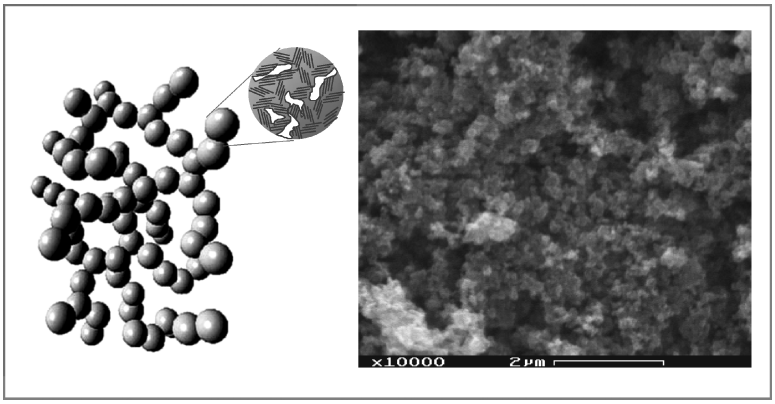

Figure 1. Model of a carbon aerogel (left) consisting of an open-porous network of microporous carbon particles; SEM picture of a carbon aerogel (right).

three-dimensional netlike, open porous backbone (Fricke and Petricevic, 2002). The constituting particles are formed upon a sol-gel process that yields the organic precursor for the carbon aerogel (Fig. 1). Their size as well as their connectivity can be tuned via the synthesis parameters. The microporosity is introduced upon the pyrolytic conversion of the organic precursor into a carbon aerogel. During that step the morphology on the meso- and macro scale is essentially preserved (Fricke and Petricevic, 2002).

To evaluate the gas adsorption dynamics we systematically varied the macropore characteristics of the monolithic carbon aerogels to allow for the separation of different contributions to the sorption dynamics. For independent structural characterization of the carbons on the macro—as well as on the micropore scale, we applied small angle X-ray scattering (SAXS). This technique is complimentary to gas adsorption analysis since it detects all porosity regardless of its accessibility. For instance Saliger et al. (2000) as well as Barbieri et al. (2001) pointed out that part of the microporosity in carbon aerogels as detected by small angle X-ray scattering is not accessible to probing molecules like nitrogen in sorption analysis.

2. Materials

The carbon aerogels were obtained from sol-gel derived organic precursors via pyrolysis at 1050°C (see also Saliger et al., 2000; Fricke and Petricevic, 2002). The porosity of the organic precursors was adjusted by the mass ratio of resorcinol and formaldehyde (39 vol%) in the starting aqueous solution (molar ratio of resorcinol: formaldehyde = 1:2); for the samples presented the ratio was set to 30 wt.% resulting in a carbon aerogel density of about 0.3 g/cm^3 (see Table 1). At fixed mass ratio the meso- and macrostructure of the organic gels was varied via the amount of sodium carbonate catalyst added to the starting solution and by changing the time that the gelling sol was kept at room temperature prior to further aging of the samples at 90°C. After aging,

Table 1. Structural characteristics as derived from SAXS-data according to Eqs. (1)–(5), with V_{micro}/m the specific micropore volume, S/m_{particle} the external specific surface area of the microporous particles and d_{mesopore} and d_{particle} the average diameter of the mesopores and the particles, respectively. On the right hand side of the table the results of the adsorption analysis with nitrogen at 77 K and carbon dioxide at 273 K are given for comparison.

Sample	Density (g/cm^3)	V_{micro}/m (cm^3/g)	$(S/m)_{\text{particle}}$ (m^2/g)	d_{mesopore} (nm)	d_{particle} (nm)	$N_2 : V_{\text{micro}}$/m (cm^3/g)	$CO_2 : V_{\text{micro}}$/m (cm^{3}g)
A4	0.327	0.27	1.7	5409	2698	na	0.24
A0	0.309	0.29	17.9	550	261	0.24	0.30
B0	0.335	0.36	155.1	55	33	0.20	0.26

the water in the pores of the aquagels was replaced by acetone prior to slowly drying the samples at 50°C and ambient pressure.

The samples denoted by A and B were prepared with a molar ratio of resorcinol to catalyst of 1500 and 1000, respectively. The additional labels "0" and "4" indicate the number of days that the samples were kept at room temperature during gelation and aging (Table 1).

3. Methods

3.1. Small Angle X-ray Scattering

Small angle X-ray scattering was performed at the beam-line JUSIFA at the German synchrotron source HASYLAB, Hamburg. The wave-vector range covered by the experiment was $0.15\ \mathrm{nm}^{-1} < q < 8\ \mathrm{nm}^{-1}$. To determine the scattering cross section for the sample investigated on an absolute scale, the scattering of the sample was calibrated using a glassy carbon standard as a reference.

The scattering of a system consisting of "highly diluted" microporous particles (see Fig. 1) can be approximated by the sum of the scattering of the envelope surface area of the microporous particles (radius R_{particle}) and the interface between the micropores and the carbon, i.e. the geometrical micropore surface. For $q \gg 1/R_{\mathrm{particle}}$ the total scattering cross section can be written as (e.g. Barbieri et al. (2001))

$$\frac{1}{m}\left[\frac{d\sigma}{d\Omega}\right]_{\mathrm{total}} = \left(\frac{1}{m}K_{\mathrm{particle}} \cdot q^{-4} + \frac{a}{(1+b^2 \cdot q^2)^2}\right) \tag{1}$$

$$\text{with} \quad \frac{K_{\mathrm{particle}}}{m} = 2\pi \cdot \rho_{\mathrm{particle}}^2 \cdot C^2 \cdot (S/m)_{\mathrm{particle}}. \tag{2}$$

The mass specific Porod-constant K_{particle}/m is relating the asymptotic q^{-4}-decay of the scattering in the intermediate q-range ($1/R_{\mathrm{particle}} \ll q \ll 1/R_{\mathrm{micro}}$, with R_{micro} the radius of the micropores) to the envelope surface area $(S/m)_{\mathrm{particle}}$ of the microporous particles with mass density ρ_{particle}. The constant $C = 8{,}504 \cdot 10^{11}$ m/kg connects the mass density of the scattering entities to the corresponding scattering cross section.

The second term in Eq. (1) describes the scattering of the micropore/carbon interface. While the parameter b is proportional to the characteristic extension of the scattering entities (here: the micropores), the weighted integral over this term, the so-called invariant Q, allows for a calculation of the total specific pore volume V_{micro}/m of the micropores and the density of the microporous particles ρ_{particle}, respectively:

$$\frac{V_{\mathrm{micro}}}{m} = \frac{1}{\rho_{\mathrm{particle}}} - \frac{1}{\rho_{\mathrm{Carbon}}} \quad \text{and} \tag{3}$$

$$\rho_{\mathrm{particle}} = \rho_{\mathrm{carbon}} - \frac{Q}{2\pi^2 \cdot C^2} \quad \text{with} \tag{4}$$

$$Q = \int_0^\infty \frac{1}{m}\left[\frac{d\sigma}{d\Omega}\right]_{\mathrm{micro}} \cdot q^2 dq = \int_0^\infty \frac{a \cdot q^2}{(1+b^2q^2)^2} dq = \frac{\pi \cdot a}{4 \cdot b}. \tag{5}$$

Hereby is m the mass of the sample contributing to scattering and ρ_{carbon} the mass density of non-porous amorphous carbon ($\rho_{\mathrm{carbon}} = 2.2\ \mathrm{g/cm^3}$).

3.2. Sorption Analysis

For sorption analysis two volumetric (manometric) sorption instruments were applied:

- ASAP2000 (with ASAP2010 software) by Micromeritics: Sorption analysis at 77 and 273 K .
- an instrument (DIPY) designed and built by the Wuerzburg University group for operation above 273 K only; this instrument is operated similar to commercial sorption instruments, however, it is equipped with an additional interferometric pressure sensor, that provides a time resolution of the pressure signal on the order of 100 ms (Reichenauer et al., 2002).

Prior to each sorption run the sample was degassed under vacuum at a temperature of 300°C (ASAP) and 200°C (DIPY), respectively, for several hours. Measurements were performed with nitrogen at 77 K (ASAP) as well as with CO_2 at 273 K (ASAP) and 296 K (DIPY), respectively. For the dynamic measurements with CO_2 cylindrical monolithic samples with a diameter of about 1.6 cm and a height of 1 cm were applied.

4. Results

4.1. Structure

Figure 2 shows the SAXS data for the three carbon aerogels investigated. While the hump in the micropore

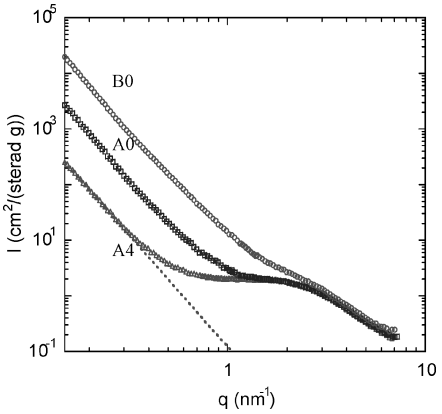

Figure 2. SAXS data for the three carbon aerogels investigated. The dashed line indicates the q^{-4}-decay of the scattering at small q values.

range (at large q values) is almost identical for all samples the slopes at small q values, reflecting the external surface area of the microporous carbon particles, are significantly different. The structural properties as derived from the SAXS data are summarized in Table 1.

4.2. *Adsorption Kinetics*

Figure 3 shows the adsorption kinetics of CO_2 at 296 K, plotted in terms of the volume adsorbed ΔV (as a result of a small change in gas pressure Δp) vs. the square root of time. This representation allows to distinguish different kinetic contributions since

$$\frac{V_{\text{ads}}(t)}{V_{\text{ads},\infty}} \approx 1 - c \cdot \sqrt{D \cdot t} \tag{6}$$

approximates the solution of the diffusion equation (see e.g. Stumpf et al. (1992)) for $0.3 < V_{\text{ads}}/V_{\text{ads},\infty} < 0.6$; hereby c is a constant characteristic for the geometry of the sample and D is the effective diffusion coefficient. The sqrt(t)-representation reveals two regimes for all samples; at short times the kinetics of adsorption is significantly different for the three aerogels, while for sqrt(t) > 7 s, the rate of adsorption is very similar. The pressure dependence of the adsorption kinetics for sample A0 is plotted in Fig. 4.

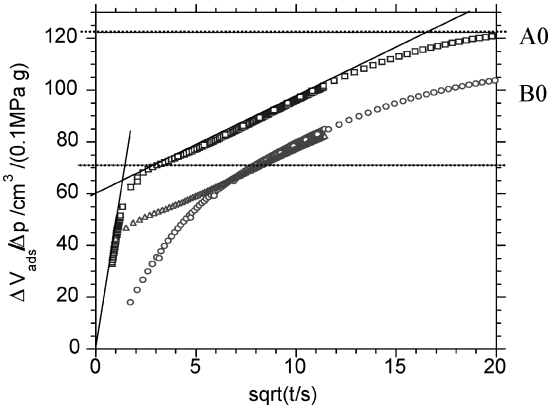

Figure 3. CO_2 adsorption curves for the three aerogels investigated as a function of sqrt(t). Symbols correspond to the ones used in Fig. 2. The full lines indicate the two ranges for the uppermost curve, in which the amount adsorbed increases linearly with sqrt(t); the dashed horizontal lines indicate the equilibrium values $V_{\text{ads},\infty}$ corresponding to the two different slopes.

5. Discussion

According to the results of the structural investigations the three highly porous hard carbons investigated display significantly different particle and macropore sizes at a similar total porosity of about 85%. The micropore volume derived from SAXS is larger or equal to the one detected by CO_2 adsorption (Table 1) as expected when comparing a method that is sensitive to all pores with one that detects accessible ones only. The values derived from N_2 adsorption analysis at 77 K are significantly lower than the results for CO_2, a behavior that is usually interpreted as restricted diffusion. The CO_2 adsorption kinetics, however, clearly reveal two adsorption steps: The fast step accounts for about 1/3 of the total micropore volume detected (Fig. 4); its kinetics highly depends on the morphology of the sample under investigation. Although the results of the fit (Fig. 4 (left)) have not yet been evaluated in detail, it seems like the rate of adsorption is controlled by gas phase transport through the macropores in combination with surface diffusion along the external surface of the microporous particles. In contrast, the kinetics of the second step neither depends on the sample morphology (pore/particle size) nor on the macroscopic sample size. Obviously, the adsorption dynamics in this case is controlled by local effects on the micropore scale. The characteristic energy for the slower adsorption component is smaller than for the fast one; according to Stöckli et al. (1990) the pore width of the micropores corresponding to the slow kinetics is therefore larger than the pore width related to the rapid adsorption step (0.55 nm compared to 0.41 nm). This leaves two explanations

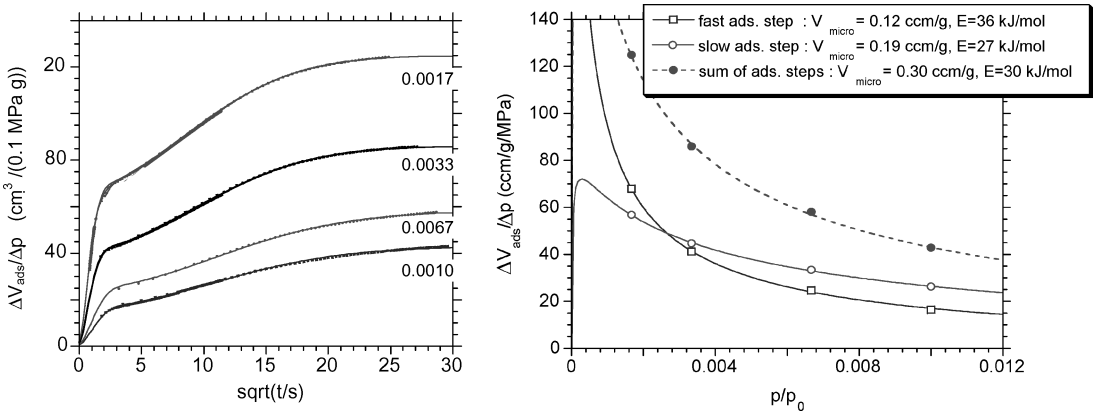

Figure 4. CO_2 adsorption curves for aerogel A0 (left). The parameters given are the average relative pressures during the individual dynamic adsorption experiments. The continuous lines represent the fit of a superposition of two adsorption steps (solution of the diffusion equation for a cylindrical body, see e.g. Stumpf et al., 1992) to the experimental points. The four fit parameters are the diffusion coefficients and the amount $V_{\text{ads},\infty}$ adsorbed for each of the two adsorption steps (see also Fig. 3). The parameters $V_{\text{ads},\infty}$ as derived from the fit in the left plot are shown as a function of the relative pressure in the right plot. The data are fitted with the derivative of a Dubinin-Radushkevich equation to yield the characteristic energy E and the specific micropore volume V_{micro}. The characteristic energies of 36 and 27 kJ/mol correspond to a radius of gyration of the related micropores of 0.41 and 0.55 nm, respectively.

for the observed behavior: The slow adsorption kinetics is either due to micropores with narrow entrances as suggested by Nakashima et al. (1995) or is related to a swelling of the carbon backbone upon CO_2 adsorption as observed for other types of carbons (e.g. Gondy and Ehrburger, 1997 or Rodriguez and Lemos de Souza, 2002); in the latter case additional micropore volume is created by an increase of the width of the micropores during adsorption analysis. The fact that in case of sample B0 the adsorptive uptake is shifted significantly to larger times indicates that the two sorption steps are not completely independent (e.g. sequential effect); due to the fast first step this behavior is not visible for the other two samples.

6. Conclusions

Investigations of the time dependence of CO_2 adsorption in the micropores of sol-gel derived highly porous hard carbons with different morphology on the macropore scale reveal two different types of micropores characterized by different adsorption kinetics. The observed behavior can in part be explained in terms of narrow restrictions at the entrance of the one type of micropores. The experiments, however, provide additional information that point toward a sequential filling of the two types of micropores like one would expect in case of a swelling of the sample upon adsorption. Future experiments that investigate the swelling in-situ during adsorption analysis will help to confirm or exclude this hypothesis.

References

Alcaniz-Monge, C. et al., *Carbon*, **40**, 541 (2002).
Barbieri, O. et al., *Journal of Non-Crystalline Solids*, **285**, 109–115 (2001).
Fricke, J. and R. Petricevic, *Carbon Aerogels, Handbook of Porous Solids*, F. Schüth, K. Sing, and J. Weitkamp (Eds.), Wiley-VCH, Weinheim, 2002, pp. 2037–2062.
Gondy, D. and P. Ehrburger, *Carbon*, **35**, 1745 (1997).
Nakashima, M. et al., *Carbon*, **33**, 1301 (1995).
Przepiorski, J. et al., *Applied Surface Science*, **196**, 296 (2002).
Reichenauer, G. et al., "Monitoring Fast Pressure Changes in Gas Transport and Sorption Analysis," *Studies in Surface and Catalysis* Vol. 144, F. Rodriguez-Reinoso, B. McEnaney, J. Rouquerol, and K. Unger (Eds.), Elsevier Science B.V. 2002, p. 443.
Rodriguez, C.F. and M.J. Lemos de Sousa, *International Journal of Coal Geology*, **48**, 245 (2002).
Saliger, R. et al., "Evolution of Microporosity upon CO_2-Activation of Carbon Aerogels," *Characterization of Porous Solids V*, Unger K.K. et al. (Eds.), 2000, p. 381.
Stöckli, et al., Carbon, **28**, 907 (1990).
Stumpf, C. et al., *Journal of Non-Crystalline Solids*, **145**, 180 (1992).
Yang, R.T., *Gas Separation by Adsorption Processes*, Imperial College Press 1997, pp. 5, 269 et seq.